Proceedings of the 26th International Conference on
Port and Ocean Engineering under Arctic Conditions
June 14-18, 2021, Moscow, Russia

A CONSTITUTIVE MODEL FOR SEA ICE: PHYSICAL BASIS, FORMULATIONS, EXAMPLES AND APPLICATIONS

David M. Cole
Engineer Research and Development Center-Cold Regions Research and Engineering Laboratory (Ret.), 72 Lyme Rd., Hanover, NH 03768, USA

ABSTRACT

This presentation outlines the physical basis for a constitutive model for ice, with emphasis on sea ice applications. The elastic, anelastic (e.g., viscoelastic) and viscous components of the model are quantified in terms of the underlying deformation mechanisms. Microstructural, temperature and salinity effects on the constitutive behavior receive attention. A time domain formulation is presented that employs a stepwise hereditary integral formulation for the anelastic components applicable to strain- or stress-controlled experiments with nonperiodic loading paths.

The model has been employed successfully in the analysis laboratory cyclic loading experiments on dry isothermal ice specimens as well as floating specimens with a naturally occurring temperature gradient. Other applications include quantifying energy dissipation during wave propagation in sea ice covers and a finite element implementation has been carried out. Additionally, the model adequately simulates an unusually high anelastic component of deformation observed during ramp loading experiments on damaged ice. Those experiments are described and the potentially important implications of this finding to the analysis of ice-induced vibrations are examined.

KEY WORDS: Ice mechanics; Constitutive model; Dislocations; Deformation mechanisms

INTRODUCTION

A wide range of contemporary research and engineering problems require a detailed understanding of the constitutive behavior of common forms of ice. The model discussed herein was developed to meet this requirement. It is based on physical mechanisms that have been observed to operate in virtually all forms of polycrystalline terrestrial ice and it captures important details of the microstructural, stress and temperature dependencies of constitutive behavior that are missed by simpler empirical approaches. Moreover, the dislocation-based anelasticity in the model proves valuable in the interpretation of the results of experiments on heavily damaged ice in which a substantial level of anelastic strain was observed after a stress drop. This phenomenon is of interest because it offers a mechanism by which damaged but intact ice can store strain energy during load-up and subsequently transfer it to a structure after a stress drop. As such, it has important implications in the analysis of ice-induced vibrations of structures. Example results are presented and evaluated in terms of the underlying dislocation mechanics. Consideration is given to the relationship between microstructure and ductility.

OVERVIEW OF THE MODEL

The model includes elastic (ε_{elas}), anelastic (ε_{ane}^{d} and ε_{ane}^{gb} associated with dislocations and grain boundaries, respectively) and viscous (ε_{visc}) components of strain. The physical bases of

these components appear in Cole (1995, 2004) and Cole and Durell (1999, 2001). Recent developments (Cole, 2020), extended the range of validity to temperatures from -50° to -0.01°C. With regard to stress and grain size, as of this writing the model is applicable up to the onset of the ductile-to-brittle transition – basically when cracking activity causes a measurable reduction in the commonly observed ductile regime failure strain of ≈ 0.01. The model is generally applicable for grain sizes ≥ 1 mm and pressure ≤ 20 MPa since deformation mechanisms not captured by the model begin to operate outside of those limits.

The unrelaxed modulus of sea ice is a function of crystallography, brine and gas porosity and temperature. The model has two mechanisms of anelasticity (associated with basal plane dislocations and grain boundaries) and each has a distribution in relaxation time and a unique activation energy. The strength of the dislocation relaxation depends on the mobile dislocation density on the basal planes and the average resolved shear stress on the basal planes. The viscous strain is based on basal dislocation drag as the rate-controlling mechanism and depends on the mobile dislocation density, temperature and the resolved shear stress on the basal planes.

The elastic and viscous components of strain are straightforward to calculate, but the two anelastic (or viscoelastic) components are time- and therefore history-dependent and require the calculation of hereditary integrals. This can be accomplished by summing the response to a series of stress or strain steps which occur at a fixed time interval.

One of the distinguishing features of the model is that both the effective activation energy and the stress exponent depend on the extent to which new dislocations are produced during straining. Consequently, the net temperature dependence is the sum of the activation energy associated with the dislocation production process and that associated with basal dislocation glide. The effective activation energy can thus range from 0.55 eV to ≈ 1 eV depending on the extent of dislocation production. Accompanying this transition in activation energy is a shift in the stress dependence from linear to an n = 3 power law. Thus, when the stress is equal to or below that required to produce new dislocations, the viscous strain rate is linear in stress. A transition to an n = 3 power law occurs as the population of new dislocations increases substantially above the pre-deformation value. In practical terms, this means that sea ice can potentially exhibit linear viscous behavior for creep stress levels up to 0.1 – 0.2 MPa.

The initial value of a specific specimen's dislocation density can be estimated from its response to a few cycles of a low stress level. To simulate generic behavior, an estimate of the initial dislocation density can be based on the type and growth history of the ice of interest.

Strain-controlled experiments can be simulated with the following form of the model:

$$\sigma_n = \sum_{i=1}^{n} \frac{\Delta\varepsilon_i}{\left(\frac{1}{E} + \delta D^d \varphi^d(t) + \delta D^{gb} \varphi^{gb}(t) + C_{visc}\Delta t\right)} \qquad [1]$$

In Eq. [1], δD^d and δD^{gb} are the strengths of the dislocation and grain boundary relaxations, respectively. φ^d and φ^{gb} are the normalized creep relaxation functions for each mechanism. C_{visc} is a viscous compliance as described below.

For load-controlled experiments, the following expression applies:

$$\varepsilon_n = \sum_{i=1}^{n} \Delta\sigma_i \left(\frac{1}{E} + \delta D^d \varphi^d(t) + \delta D^{gb} \varphi^{gb}(t) + C_{visc}\Delta t\right) \qquad [2]$$

The normalized creep relaxation functions are based on the frequency domain results of Cole (1995, Eq. 12). The time domain formulation substitutes $t = \omega^{-1}$ in the expression (from Cole, 1995) $s^d = \ln(\tau^d \omega)$ so $s^d = \ln(\tau^d / t)$ and $s^{gb} = \ln(\tau^{gb} \omega)$ in the creep functions

for the dislocation and grain boundary relaxation mechanisms, respectively.

$$\varphi^d(t) = 1 - \frac{2}{\pi} Tan^{-1}[\exp\left(-\alpha^d \ln(\frac{t}{\tau_d})\right)] \quad [3]$$

α^d = 0.54 and α^{gb} = 0.6 are experimentally determined relaxation peak width parameters for the dislocation and grain boundary relaxations, respectively. As a practical matter when using laboratory data with Eq. [3], a small value (e.g., 10^{-6} s) can be added to the quantity $(\frac{t}{\tau_d})$ to avoid problems when t = 0 s at the start of an experiment.

The viscous strain contribution developed in Cole and Durell (2001) is:

$$\dot{\varepsilon}_{visc} = \frac{\beta \rho \Omega^{1.5} b^2 \sigma_{creep}}{B_0} \, exp\left(-\frac{Q_{glide}}{kT}\right) \quad [4]$$

As noted above, Eq. [4] indicates that the viscous strain rate is linear in stress when the dislocation density ρ (in m^{-2}) is constant. β is a dimensionless constant = 0.3 for the ductile regime, Ω is an average Schmidt factor (= 0.32 for ice with randomly oriented grains), b is Burgers vector (4.52×10^{-10} m), B_o (= 1.205×10^{-9} Pa s) is the preexponential in the basal dislocation drag expression, Q_{glide} is the activation energy for basal glide (0.55 eV) and k is Boltzmann's constant (1.38062×10^{-23} J K^{-1}). For a fixed temperature and microstructure, it is convenient to consolidate the non-stress-related terms as follows:

$$C_{visc} = \frac{\beta \rho \Omega^{1.5} b^2}{B_0} \, exp\left(-\frac{Q_{glide}}{kT}\right) \quad [5]$$

So,

$$\dot{\varepsilon}_{visc} = C_{visc} \sigma_{creep} \quad [6]$$

The units of Eq. [6] are such that $C_{visc}\,\Delta t$ has units of compliance and is thus compatible with the other terms in Eqs. [1] and [2]. Cole and Durell (1999, 2001) give the dislocation density that evolves during creep as a function of the stress level, temperature and strain:

$$\rho(\sigma, T) = \rho_0 + f_0 f(\varepsilon_i) \left(\frac{\sigma_{creep}}{E(T)}\right)^2 exp\left(-\frac{Q_\rho}{kT}\right) \quad [7]$$

Where:

$$f(\varepsilon_i) = \frac{exp\left(\frac{\varepsilon_i}{\varepsilon_0}\right) - exp\left(-\frac{\varepsilon_i}{\varepsilon_0}\right)}{exp\left(\frac{\varepsilon_i}{\varepsilon_0}\right) + exp\left(-\frac{\varepsilon_i}{\varepsilon_0}\right)} \quad [8]$$

ε_i is the creep strain, ε_0 (= 0.005) is the strain associated with the inflection point in Eq. [7]. ρ_0 is the initial dislocation density, Q_ρ is the activation energy for dislocation production (0.45 eV), $f_o = 4 \times 10^{25}$ m^{-2} for sea ice, ε_0 is the strain associated with the inflection point in Eq. [8], σ_{creep} is the creep stress and $E(T)$ is the temperature-dependent elastic modulus. ρ_0 depends on the brine porosity and typical values for unstrained ice, for example, are in the range of 0.6 to 1.4×10^9 m^{-2} for brine porosities in the range of 4 to 8 ppt.

APPLICATIONS TO UNDAMAGED SEA AND SALINE ICE

Although it was initially developed on the basis of laboratory experiments on the scale of 0.1m, the model produced credible values of internal friction for in-situ sea ice specimens with minimum dimensions in the range of 10-30 m (Cole and Dempsey, 2001). It has been successfully applied to the strain-controlled, uniaxial, cyclic loading experiments of Heijkoop (2017) and Heijkoop et al. (2018) on laboratory-prepared saline ice specimens. Wei et al. (2020)

successfully applied Eq. [2] to the results of load-controlled cyclic compression experiments on floating blocks of laboratory-prepared saline ice. The dislocation density of each specimen was determined from its response to a low-amplitude 0.1 Hz waveform and that value was used to simulate the response to other stress levels and frequencies. Finally, the model has been employed to provide credible internal friction values in the calculation of wave attenuation in ice covers (Marchenko and Cole, 2017; Ardhuin et al., 2020).

O'Connor et al. (2020) presented a finite element implementation of the constitutive model that successfully simulated the full stress-strain behavior of saline ice under cyclic (from -10° to -50°C) and standard creep (-10°C) loading conditions, as well as staged creep and recovery experiments (-15°C) that involved variable creep stress levels and times under load. In all cases, the model produced highly credible simulations of the experiments.

APPLICATION TO DAMAGED ICE

While examining archives of unpublished laboratory experiments on granular- and columnar-grained freshwater ice in preparation for the present effort, a potentially significant phenomenon came to light. The experiments involved a series of load/unload ramps in compression on each specimen to examine the accumulation of anelastic and viscous strain with progressive microstructural damage. The loading sequence in these experiments was similar to the biaxial compression experiments on columnar-grained freshwater ice reported by Iliescu and Schulson (2002). For loading rates of 5 and 10 MPa s^{-1} at -10°C, the granular ice specimens absorbed a substantial amount of strain energy prior to failure, and the associated build-up in dislocation-based anelasticity was sufficient to produce a prominent strain peak which occurred after the peak in the applied stress. Thus, the anelastic mechanism essentially stored strain energy during loading and released it shortly after the direction of loading was reversed. This is precisely the type of process that would provide energy transfer from the ice to a structure during a rapid drop in stress during an ice-structure interaction event. The anelasticity mechanism could therefore play a key role in sustaining the motion of the structure. As shown below, calculations based on the ramp loading experiments indicate that a) this mechanism can supply sufficient strain energy to sustain IIV and b) its kinetics can be understood in terms of dislocation mechanics. Although the latter observation is surprising given the slow glide velocity of basal dislocations in ice, high stress levels and short travel distances are likely key aspects of the problem that allow it to operate on a short time scale.

Experimental details. The experiments involved the repeated application of a uniaxial compressive stress to cylindrical specimens of laboratory-prepared ice (Cole, 1978) using a closed-loop electro-hydraulic test system programmed to apply the waveform shown in Figure 1. The specimens measured 127 mm in length and 50.8 mm in diameter.

Most of the experiments employed a stress application rate in the range of 5-10 MPa s^{-1}. The peak stress increased from an initial value of ≈ 2 MPa in most cases by increments of ≈ 2-4 MPa until the specimen failed (8-11 MPa). In some cases, several successive ramps of a nominally constant peak stress were applied. The full test matrix involved temperatures of -10°, -20°, -30° and -40°C for the granular ice and -10°, -20° and -30°C for the columnar ice, with the axis of loading perpendicular to the long axis of the grains.

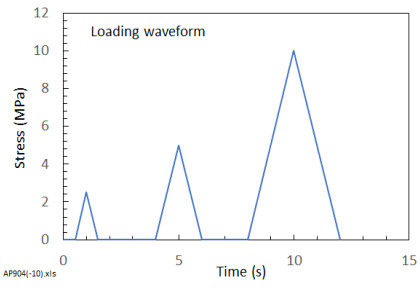

Figure 1. The waveform used in the ramp load/unload experiments.

Results of greatest interest at -10°C appear below and a full report will appear elsewhere.

The peak stress in the initial ramp was not expected to alter the specimen, as shown in the work cited above. The strain response to these ramps, as seen in Figure 2a for curves labeled *a* and *d*, reflects the initial dislocation density of 10^9 m^{-2}. Note, however, that for the curves labeled *d*, *h* and *i* in Figure 2, the hysteresis loop area increased with successive stress applications, indicating that the stress level in those ramps was sufficiently high to generate new dislocations (2.4, 5.0 and 5.5 × 10^9 m^{-2}, respectively). Figure 2b shows stress and strain vs. time for the curve labeled *i* in Figure 2a to illustrate the significant amount of strain in the initial direction of loading that occurred after the peak in the applied stress. Although photographic records are not available for these experiments, extensive microcracking accompanied the increase in dislocation density. Figure 3 shows one of the more striking examples of straining after the stress peak from the experiments at -10°C and a stress application rate of 10 MPa s^{-1}. In this case, the peak in anelastic strain lagged the stress peak by 0.5 s and the associated dislocation density was 1.15 × 10^{10} m^{-2}. Additionally, this specimen accumulated 1.92 × 10^{-2} of viscous strain in the 11 loading cycles it experienced prior to compressive failure. This is nearly two times the viscous strain (0.01) associated with ductile compressive failure under a single loading. This stands in contrast to the essentially brittle behavior of the columnar-grained specimens (e.g,, HOL6) which accumulated a total viscous strain of only 5.28 × 10^{-4} prior to its compressive failure. The associated anelastic strain was < 4 × 10^{-4}.

Modeling the ramp loading experiments. Modeling the ramp loading experiments constitutes an extrapolation of the model described above to stress levels in the vicinity of the uniaxial compressive strength. Preliminary analysis indicated that quantities in Eqs. [7] and [8], which are based on creep loading conditions for stress levels under 3 MPa, will need to be assessed for the higher stress levels and loading rates of the ramp experiments. Thus, although the model cannot currently predict the dislocation density in the ramp loading experiments, it can be used to track changes in the dislocation density based on the increasing hysteresis loop area. Figure 4 shows the results of those calculations for specimen AP904 for peak stress levels in the

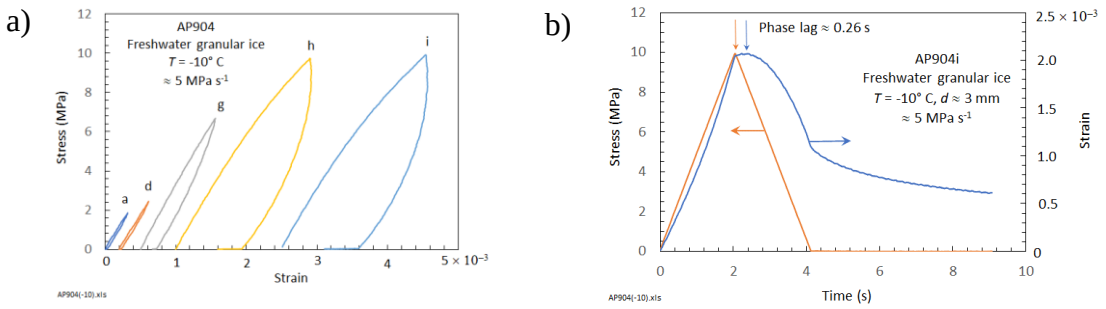

Figure 2. Example results from the ramp loading experiments on a specimen of granular freshwater ice. a) Stress-strain plots from several load cycles applied to specimen AP904 under the indicated conditions. The individual curves have been shifted along the strain axis for clarity. b) Strain and stress vs. time for the curve labeled *i* in Fig. 2a,

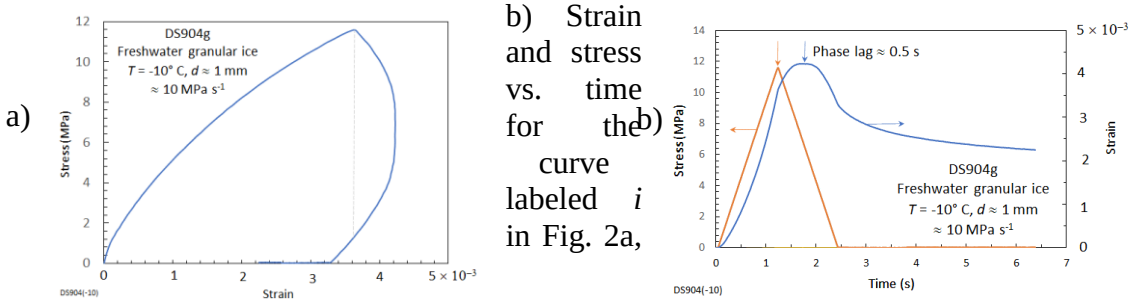

illustrating the phase lag between the peak in the applied stress and the peak in the resulting strain.

Figure 3. Example results for a 10 MPa s^{-1} ramp loading experiments. a) Stress-strain plot for specimen DS904 under the indicated conditions. The area under the curve to the right of the vertical line drawn through the peak stress is the strain energy discussed in the text. b) Strain and stress vs. time for the curve in Fig. 3a, illustrating a phase lag of ≈ 0.5 s between the peak in the applied stress and the peak in the resulting strain.

dislocation density increases in proportion to the peak stress to the 2^{nd} power, which is in keeping with observations of this relationship in polycrystalline materials in general as well as ice at much lower stress levels. This observation suggests continuity with dislocation processes known to operate at the lower stress levels and thus provides a measure of confidence that the observed behavior is indeed rooted in dislocation mechanics.

Figure 5 compares the model and experimental results in stress-strain space for which the dislocation density was determined from the hysteresis loop area. The cases in Figure 5 a and b involved minimal microstructural damage but the dislocation density did increase somewhat. It is clear from Figure 5a and b that the simulations accurately capture the ice response. The case in Figure 5c involved a higher level of viscous strain ($\approx 2.5 \times 10^{-3}$ vs. $\approx 5 \times 10^{-4}$ for the specimens shown in Fig. 5 a and b) due presumably to microcracking – a process which is not currently accounted for in the model – coupled with viscous strain due to dislocations. As an expedient, since the current form of the model does not account for microstructural damage, the viscous component of strain was increased empirically to match the experiment. The analysis of the highly damaged ice suggested that the strength of the grain boundary relaxation decreased from its typical value of 4×10^{-11} Pa^{-1} for undeformed ice. Although this relaxation mechanism has a minor effect on the overall constitutive response under the prevailing conditions, it is a point of interest for the future.

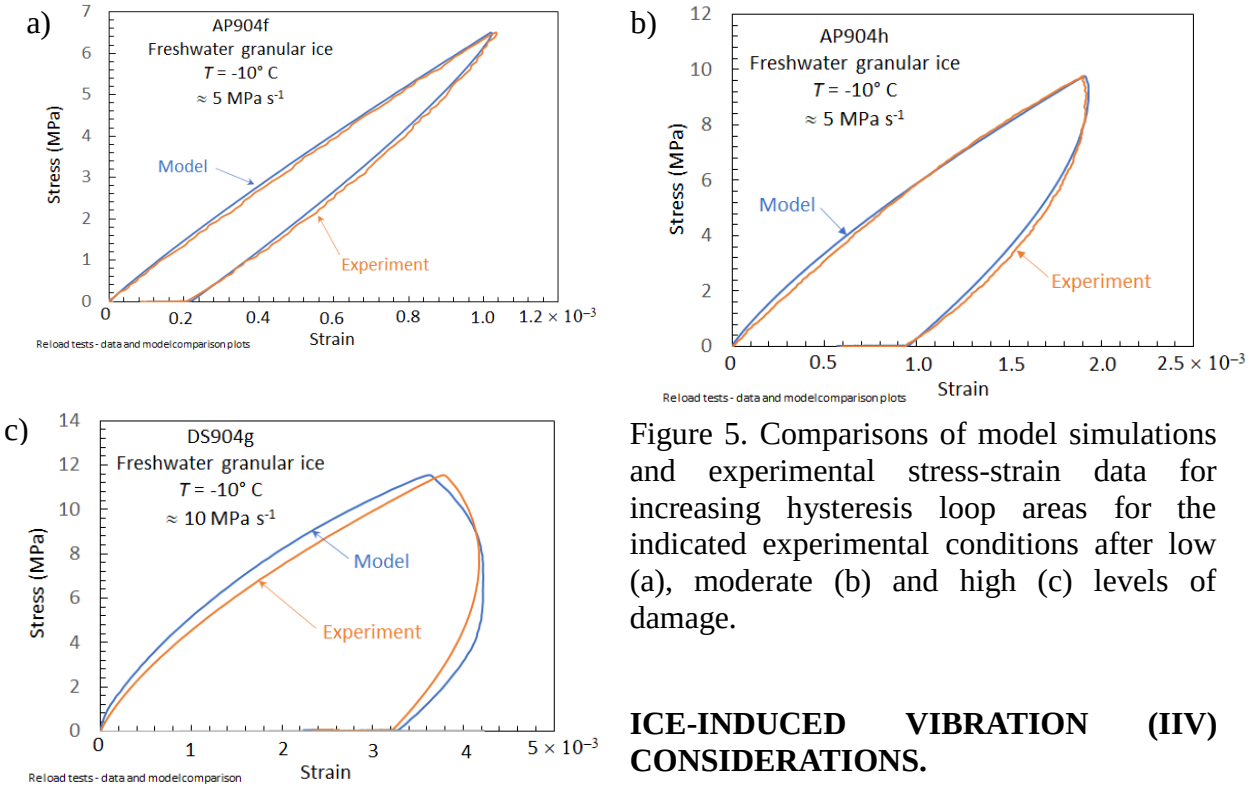

Figure 5. Comparisons of model simulations and experimental stress-strain data for increasing hysteresis loop areas for the indicated experimental conditions after low (a), moderate (b) and high (c) levels of damage.

ICE-INDUCED VIBRATION (IIV) CONSIDERATIONS.

To warrant consideration for the IIV problem, the anelasticity mechanism must provide sufficient energy to sustain structural vibrations. To address this point, H. Hendrikse (personal communication) kindly provided an estimated range of 1.05 to 14.7 *kJ* for the energy required per cycle of oscillation to sustain motion of the Norströmsgrund lighthouse (see Jochmann, 2003). The energy associated with the dislocation mechanism is estimated as the area under the stress-strain curve to the right of the peak stress (indicated by the vertical line in Figure 3a). Calculations for several ramps prior to failure for specimen DS904 (designated f, g and i) indicated that the specific strain energy increased as follows: 2.7, 4.3 and 9.3 $kJ\ m^{-3}$. The peak stress was ≈ 11.4 MPa.

The above energy values indicate that for the upper estimate of 14.7 *kJ*, a volume of damaged ice in contact with the structure of 1.6 to 5.4 m^3 would be needed to sustain IIV. This is reasonable for the Norströmsgrund lighthouse given its ≈ 7 m width and an 0.4 m thick ice sheet. These estimates give confidence that the level of strain energy provided by the anelasticity mechanism is sufficient to sustain IIV and is thus worthy of further consideration. The fact that the necessary level of anelasticity emerges only for highly damaged ice subjected to an abrupt stress drop is commensurate with the observation by Hendrikse and Metrikine (2016) that IIV requires the operation of failure by crushing in combination with a failure process that provides abrupt drops in stress.

MICROSTRUCTURAL CONSIDERATIONS AND IIV

In light of the observed differences in ductility of freshwater granular and columnar ice, the matter of inferring aspects of sea ice behavior from columnar freshwater ice experiments deserves comment. Macroscopically, both have columnar grain structures with c-axes in the horizontal plane, but the flaw structure and intrinsically higher dislocation density of sea ice leads to mechanical behavior that is fundamentally more ductile than undamaged columnar-grained freshwater ice – a fact that has significant ramifications in problems such as IIV which

are centered on the ductile-to-brittle transition.

Grown-in dislocation density and ductility. One of the stated assumptions in Määttänen's (1978) seminal work on IIV was that inelastic processes in ice were too slow to operate on the time scale of structural vibrations. That assumption, which precluded consideration of a time-dependent mechanism in the ice, was based on a statement of Gold (1977) to the effect that freshwater ice can be considered as elastic up to failure for loading times under 2s. That statement is correct for unconfined, previously undeformed columnar freshwater ice strained to failure in compression in a matter of seconds. The inelastic, and specifically anelastic, contributions to straining (even at sub-second time scales, as demonstrated above) increase significantly with damage, however, due to the associated increase in the dislocation density, so it is physically justifiable to include such processes in IIV analyses.

Although the ramp loading experiments on columnar-grained freshwater ice showed primarily brittle behavior, the experiments of Iliescu and Schulson (2002), which employed a similar load path and rates, but with a degree of biaxial confinement, exhibited significantly more ductility. The total viscous strain at failure in their experiments was in the range of 3×10^{-3} to 7×10^{-3} (values associated with the ductile-to-brittle transition in ice, see Cole, 1987), indicating that confinement promoted ductile behavior and allowed the microstructure to absorb strain energy on the scale required for the anelastic mechanism to operate.

The inherent brittleness of unstrained columnar-grained freshwater ice vs. saline ice is explained in part by the fact that its as-grown dislocation density is approximately and order of magnitude less that saline ice (Cole and Durell, 2001), which significantly reduces the extent of inelastic straining. The more ductile nature of sea ice and laboratory-prepared saline ice specimens that have the proper cellular subgrain structure is due primarily to a high grown-in dislocation density relative to columnar freshwater ice and a flaw-laden microstructure restricts the size of nucleating microcracks and arrests their propagation.

The tendency of columnar-grained freshwater ice to brittle behavior suggests that it may be difficult to achieve IIV in ice-structure interaction experiments with that ice type. This may have been a factor in the pioneering work of Sodhi (1991). He conducted indentation experiments on columnar-grained freshwater ice and examined the energy balance in the test system during creep, intermittent and continuous failure modes. He observed that energy was absorbed by failure processes in the ice in all cases but that no energy was returned to the structure from the ice. That observation, and the fact that what is referred to as lock-in behavior was never observed, led to the conclusion that the results offered no support for the theory of negative damping. In light of the foregoing observations regarding the brittleness of columnar freshwater ice, that conclusion should not be surprising. Essentially, without sufficient confinement, the brittle nature of that ice type rendered it unlikely to achieve a state of damage that can accommodate a high dislocation density and simultaneously remain in contact with the structure during stress drops.

Rate, damage and grain size effects. Regarding the topic of negative damping, that concept was applied to ice-structure interaction by Blenkarn (1970) to explain vibrations observed on structures in Cook Inlet, AK. The calculation relied on experimental observations by Peyton (1966) of a negative slope in the compressive strength-stress application rate relationship. That work showed that for stress application rates in the approximate range of 0.23 to 1 MPa s^{-1}, the compressive strength of Cook Inlet ice cores decreased from ≈ 2 to 1 MPa and the time to failure decreased from ≈ 9 to 1s. The approach of Blenkarn (1970) has been employed for decades (e.g., Määttänen, 1978; Wu and Qiu, 2019), although that particular relationship in not

universally observed, particularly for saline ice. In fact, Schwarz and Weeks (1977) noted that Peyton's experiments on cores from near Point Barrow, AK, did not exhibit the trend seen in the Cook Inlet cores when tested under the same loading rates. Additionally, there is evidence that the drop in unconfined compressive strength in the ductile-to-brittle transition in freshwater ice is associated with fine-grained material as discussed in the following paragraph.

Freshwater ice compression strength data summarized in the universal curve of Michel and Toussaint (1977) show a significant strength drop in the 10^{-3} to 10^{-2} s^{-1} order of magnitude in strain rate. The data points for S2 ice in that region are dominated by the results of Carter (1971) who reported a grain size $d \approx 4$ mm. The latter work included an additional set of results for cores from deeper in the sheet, which presumably had a larger grain size, and which showed a less abrupt transition region extending into the 10^{-4} s^{-1} order of magnitude of strain rate. The compression strength results for granular ice at -5°C in Cole (1987) show a stress drop as in Carter (1971) for fine-grained (d = 1.5 mm) specimens but virtually no drop was observed for d = 5 mm-grain-size specimens through the ductile-to-brittle transition. Meglis et al. (2000) summarized an extensive program of confined compression experiments on granular freshwater ice at -10°C with a focus on the constitutive behavior of damaged ice. Six levels of prior straining (up to 40% axial) were examined and the only results to exhibit a decrease in compressive strength through the ductile-to-brittle transition were associated with the highest level of prior straining and the drop occurred for strain rates above $\approx 10^{-1}$ s^{-1}. The results at prior strain levels of 2 to 30% showed no evidence of a decrease.

The extensive experimental work reported by Kuehn and Schulson (1993) on laboratory-prepared saline ice focused on the ductile-to-brittle transition at temperature of -5°, -10°, -20° and -40°C. The trend for compressive strength to decrease with strain rate in that work ranged from barely discernable at -10°C to significant at -40°C, at which temperature the transition extended over some 4 orders of magnitude in strain rate rather than the one order of magnitude range seen in Michel and Toussaint (1977). It is thus evident that the ice strength-strain rate relationship is considerably more varied in the magnitude of the drop and the range of strain rates over which it occurs than seen in the universal curve of Michel and Toussaint (1977).

The work of Stone et al. (1997) shows some common features with the results from the ramp loading experiments presented above. They reported strain energy density values of ≈ 5 $kJ\ m^{-3}$ for specimens that had been damaged under a 20 MPa confining pressure and subsequently subjected to load pulses up to 7 MPa. Additionally, the anelastic strain values discerned from their data plots are in the 10^{-3} order of magnitude, as found in the ramp loading experiments. The facts that both the strain energy density and anelastic strain values for the same ice microstructure reported by Stone et al. (1997) are in good agreement with the present ramp loading experiments provides some assurance of similar underlying dislocation mechanics.

In light of the above, it is evident that microstructure and damage influence the mechanical behavior of ice in the critical ductile-to-brittle transition region and that dislocation mechanics can play an important role in the constitutive behavior to relatively high strain rates.

DISCUSSION

It is evident that a physics-based constitutive model provides a useful tool for analyzing and modeling the constitutive behavior of sea ice. To simulate the response of a specific specimen, the model requires input regarding its physical properties and loading conditions and the initial dislocation density can be determined from its response to several cycles of a low stress. The model can be queried to determine the response (internal friction, for example) of generic microstructures under specified loading conditions for use in other applications.

The results of the ramp loading experiments suggest that dislocation-based anelasticity in damaged ice is worth considering as a component in the modeling of ice-structure interaction in general and IIV in particular. Although details of the rate and temperature dependence of damage accumulation and dislocation density build-up require further study, it is evident that dislocation-based anelasticity can operate on the requisite time scale and produce sufficient strain energy to sustain IIV. Moreover, the kinetics of basal dislocations are reasonably well understood, and methods are available to quantify the above-mentioned dependencies, so a quantitative treatment of the topic is completely within reach.

Another point for further consideration is that the anelasticity mechanism could be explored in-situ by instrumenting both the ice and the structure in an IIV experiment. When the anelasticity mechanism operates, the phase lag between the peak stress and the peak strain was as high as 0.25 to 0.5 s – which should be relatively straightforward to detect in an experiment. Such measurements would provide a means to establish whether or to what extent the anelasticity of the ice is playing an active role in the interaction process. Note that when global ice loads are determined from the structure's movement, the critical phase relationship between the force in the ice and the deformation of the structure is lost.

Regarding the applicability and implementation of the anelastic straining mechanism, it will be critical to establish with experiments whether the microstructure of a specific ice type can absorb a sufficient amount of strain energy and build up the necessary dislocation density to allow the anelastic mechanism to operate effectively. Ideally, such experiments should be conducted over a range of temperature, stress application rates and boundary conditions. Although implementation in an existing modeling framework is never trivial, approaches such as that taken by Hendrikse and Metrikine (2016a, b) and Hendrikse et al. (2018), which incorporate a basic multi-component rheological ice model, provide the necessary framework to implement a physics-based ice rheology of the type described above.

CONCLUSIONS

1. From the foregoing, it is evident that the physics based model presented adequately captures the constitutive behavior of freshwater and sea ice under dry isothermal conditions and floating sea and saline ice with a naturally occurring temperature gradient.
2. Experimental results were presented which showed clear evidence that fine-grained granular freshwater ice subjected to damage by repeated uniaxial compressive load ramps in the range of 5-10 MPa s^{-1} at -10°C exhibits an unusually high level of anelastic strain.
3. An analysis of the constitutive behavior of the damaged ice specimens led to the conclusion that the observed anelasticity is due to dislocations and can be modeled as such.
4. Preliminary calculations of the strain energy available from the anelasticity mechanism during a stress drop suggest that it is sufficient to support IIV.
5. The strain dependence of the dislocation density evolution under ramp loading conditions varies from that observed under creep loading conditions and requires further study.

ACKNOWLEDGEMENTS

Mr. Glenn Durell of ERDC-CRREL (Ret.) conducted the experiments. As always, his help and cheerful professionalism are greatly appreciated. The author is indebted to Prof. Hayo

Hendrikse, Department of Hydraulic Engineering, Delft University of Technology for helpful discussions and for providing estimates of the energy required to sustain the IIV observed for the Norströmsgrund lighthouse. The author is grateful to Dr. Devinder Sodhi (ERDC-CRREL Ret.) for helpful discussions and providing insight into his experimental findings.

REFERENCES

Ardhuin, F., Otero, M., Merrifield, S., Grouazel, A., Terrill, E., 2020. Ice breakup controls dissipation of wind waves across Southern Ocean sea ice. *Geophys. Res. Lett*., 47(13) https://doi.org/10.1029/2020GL087699

Cole, D.M., 2020. On the physical basis for the creep of ice: the high temperature regime. *J. Glaciol.*, 66(257) 401- 414 DOI: https://doi.org/10.1017/jog.2020.15

Cole, D.M., 2004. A dislocation-based model for creep recovery in ice. *Phil. Mag*., 84(30), 3217-3234

Cole, D.M., 2003. A dislocation-based analysis of the creep of granular ice: preliminary experiments and modeling. *Annals of Glaciol*., 37, 18-22

Cole, D.M., 2001. The microstructure of ice and its influence on mechanical properties. *Engineering Fract. Mech*., 68, 1797-1822

Cole, D.M., 1998. Modeling the cyclic loading response of sea ice. *Int'l. J. Solids and Struct.*, 35(31-32), 4067-4075

Cole, D.M., 1995. A model for the cyclic loading of saline ice subjected to cyclic loading. *Phil. Mag. A*, 72(1), 231-248

Cole, D.M. and J.P. Dempsey, 2001. Influence of scale on the constitutive behavior of sea ice. In *IUTAM Symp. on Scaling Laws in Ice Mechanics and Ice Dynamics, Solid Mechanics and its Applications*, Vol. 94, Kluwer Academic Publishers, Boston, 251-264

Cole, D.M. and Durell, G.D., 2001. A dislocation-based analysis of strain history effects in ice. *Phil. Mag. A.* 81(7), 1849-1872

Cole, D.M. and Durell, G.D., 1999. Strain history effects on the anelastic and viscous straining of saline ice. *Intl. Assoc. Hyd. Res., 14th Intl. Ice Symp*., II, 989-994

Gold, L.W., 1977. Engineering properties of fresh-water ice. *J. Glaciol.*, Vol. 19, No. 81, pp. 197-211

Heijkoop, A.-N., 2017, Sea ice subjected to cyclic compression: Laboratory experiments and a dislocation based model. M Sci Thesis, Delft Univ. of Technol. 110p

Heijkoop, A.-N., Nord, T.S. and Høyland, K.V., 2018. Sea ice subjected to cyclic compression. *Proc. 24th Intl. Assoc. Hydraulic Res. Intl. Symp. on Ice,* Vladivostok, 118-127, ISSN 2414-6331

Hendrikse, H. and Metrikine, A., 2016a, Edge indentation of ice with a displacement-controlled oscillating cylindrical structure. *Cold Reg. Sci. Technol*., Vol. 121, 100-107

Hendrikse, H. and Metrikine, A., 2016b. Ice-induced vibrations and ice buckling. *Cold Reg. Sci. Technol.*, 131, 129-141

Hendrikse, H., Ziemer, G. and Owen, C.C., 2018. Experimental validation of a model for prediction of dynamic ice-structure interaction. *Cold Reg. Sci. Technol*., 151, 345-358

Iliescu, D. and Schulson, E.M., 2002. Brittle compressive failure of ice: monotonic versus cyclic loading. *Acta Materialia*, 50, 2163-2172

Ji, X. and Oterkus, E., 2018. Physical mechanism of ice-structure interaction. *J. Glaciol*., 64(244), 197-207

Jochmann, P., 2003. STRICE REPORT: Full Scale Measurements at Lighthouse Norströmsgrund – Winter 2001 ¨ –. Tech. Rep. Deliverable No. D-5.1.1, Hamburgische Schiffbau-Versuchsanstalt GmbH, Hamburg.

Kuehn, G.A. and Schulson, E.M., 1993. The mechanical properties of saline ice under uniaxial

compression. *Ann. Glaciol*., 19, 39-48
Marchenko, A. and Cole, D.M., 2017. Three physical mechanisms of wave energy dissipation in solid ice. *Proc. 24th Intl. Conf. on Port and Ocean Engin. under Arctic Conditions*, June 11-16, Busan, Korea. POAC17_086_Aleksey.pdf
Meglis, I.L., Barrette, P.D., Ho, H. K. and Jordaan, I.J., 2000. Triaxial Testing of Freshwater Ice 1992-1998, PERD/CHC REPORT 75-13 Extended version, Ocean Engineering Research Centre, Memorial University of Newfoundland, St. John's, NF, Canada.
Michel, B. and Toussaint, N., 1977. Mechanisms and theory of indentation of ice plates. *J. Glaciol.*, 19(81), 285-300
O'Connor, D., West, B., Haehnel, R., Asenath-Smith, E. and Cole, D.M., 2020. A viscoelastic integral formulation and numerical implementation of an isotropic constitutive model of saline ice. *Cold Reg. Sci. Technol*., 171 102983 https://doi.org/10.1016/j.coldregions.2019.102983
Schulson, E.M., 2006. The fracture of water ice Ih - A short overview *Meteoritics & Planetary Science.* 41(10), 1497-1508
Schwarz, J. and Weeks, W.F., 1977. Engineering properties of sea ice. *J. Glaciol*., 19(81), 499-531
Sodhi, D.S., 1991. Energy exchanges during indentation tests in fresh-water ice. *Ann. Glaciol*., 15, 247–253
Stone, B.M., Jordaan, I.J., Xiao, J. and Jones, S.J., 1997. Experiments on the damage process in ice under compressive states of stress. *J. Glaciol.*, 43(143), 11-25
Wei, M., Polojärvi, A., Cole, D.M., Prasanna, M., 2020. Strain response and energy dissipation of floating saline ice under cyclic compressive stress. *The Cryosphere* 14, 2849–2867
Wu, T. and Qiu, W., 2019. A dynamic ice-structure interaction model for prediction of ice-induced vibration. *Periodica Polytechnica Civil Engineering*, 63(2), 550-561. https://doi.org/10.3311/PPci.13080